Catalytic Oxidation of Soot and Volatile Organic Compounds over Cu and Fe Doped Manganese Oxides Prepared via Sol-Gel Synthesis

2021-24-0088 Published 05 Sep 2021

# Catalytic Oxidation of Soot and Volatile Organic Compounds over Cu and Fe Doped Manganese Oxides Prepared via Sol-Gel Synthesis

**Miguel Jose Marin Figueredo, Marco Piumetti, Debora Fino, Nunzio Russo, Clarissa Cocuzza, and Samir Bensaid** Politecnico di Torino

***Citation:*** Marin Figueredo, M.J., Piumetti, M., Fino, D., Russo, N. et al., "Catalytic Oxidation of Soot and Volatile Organic Compounds over Cu and Fe Doped Manganese Oxides Prepared via Sol-Gel Synthesis," SAE Technical Paper 2021-24-0088, 2021, doi:10.4271/2021-24-0088.

## Abstract

A set of manganese oxide catalysts was synthesized and doped with Cu and/or Fe by means of the citric acid sol-gel preparation method. The samples were studied by means of several characterization techniques: field-emission scanning electron microscopy (FESEM), X-ray powder diffraction (XRD), $N_2$-physisorption at -196 °C, $H_2$ and soot temperature-programmed reduction ($H_2$-TPR, soot-TPR) and X-ray photoelectron spectroscopy (XPS). The catalytic performance of the prepared catalysts was investigated in the oxidation of a probe VOC molecule (propylene) and carbon soot singularly and simultaneously. The catalytic performances were studied as well assuring a content of 5 vol.% of water in the gaseous reactive mix. The investigations evidenced that the best soot catalytic oxidation rates occurred over the $Mn_2O_3$ sample, while the copper-doped manganese oxide (*i.e.* the $MnCu_{15}$) showed the best performance in the decomposition of propylene. The soot conversion rates of the samples were positively correlated to the $Mn^{3+}/Mn^{2+}$ ratio of the samples, while the activity in the oxidation of propylene could be attributed to the reducibility enhancement caused by the insertion of Cu species in the structure of $Mn_2O_3$. The most active samples in soot oxidation demonstrated only a slight catalytic activity deactivation after thermal aging and practically no deactivation during the tests with humidity. Interestingly, the simultaneous soot-propylene oxidation tests evidenced an enhancement of the oxidation of soot particles in "tight" contact with the catalyst, likely due to a cooperative effect between soot and propylene oxidation.

## Introduction

Nowadays, there is an increasing concern about the air quality standards. Consistently, stringent regulations concerning the amount of pollutants (*e.g.* carbonaceous particulate matter, volatile organic compounds, etc.) present in ambient air are being applied around the globe [1, 2]. The production of carbonaceous particulate matter may take place in the industry and during daily common activities (*e.g.* driving of vehicles) as well [3]. The particulate matter consists in aggregates of elemental carbon (*i.e.* soot), along with organic compounds adsorbed on its surface, metal oxides and sulphur. The soot is formed as the result of the combustion of hydrocarbons in a stream with a deficient composition of oxygen. Therefore, the pyrolysis of hydrocarbons takes place during this process and is followed by the nucleation of solid particles, surface growth, coalescence and finally their agglomeration [4, 5].

The abatement of particulate matter has been studied using different transition metal oxide catalysts (*e.g.* manganese oxides, copper oxide and iron oxide) [6-8]. Some of these metals are among the most abundant in the earth and thus represent interesting resources for the production of sustainable catalysts [9]. The literature evidences that several parameters regarding the catalyst influence on the efficiency of the particulate matter oxidation process (*e.g.* solid-solid phases contact, nanostructure, reducibility, etc). The solid-solid contact between the catalyst and the soot is a paramount condition that affects the effectiveness of a catalyst. A "loose contact" between soot and the catalyst may be achieved by gently mixing the powders with a spatula for a short time (ca. 1-2 min). This procedure allows to homogenize the powder mixture and grants the obtention of reproducible catalytic results. Furthermore, it assures contact dynamics more representative of the real operative conditions in particulate filters. On the other hand, the soot-catalyst "tight contact" condition is obtained by performing a ball-milling of the powders. This procedure assures a highly intimate contact between the soot and the catalyst and maximizes the overall soot-catalyst contact points. Consistently, it can be a way to discriminate better the activity of the catalytic surface of the samples [10, 11]. As well, the literature evidences that the nanostructure plays an important role in the oxidation of soot. This is related to an increase of the catalyst-soot points of contact in

well-defined nanostructures (*e.g.* nanocubes, nanorods) and the elevated presence of highly catalytically active surfaces. Instead, when these parameters are not optimized (*i.e.* in nanopolyhedra structures) the catalytic performance of the catalysts could be less promising [12, 13].

In this research work a set of manganese doped oxides were synthesized via a sol-gel procedure using citric acid and metal nitrates. The mesoporous powder catalysts prepared using this technique evidenced a good catalytic activity in the abatement of particulate matter in loose contact conditions. As well, the catalysts were tested in the abatement of propylene as VOC probe molecule. It is known that the diesel exhaust may contain not only particulate matter, but it may contain as well a discrete amount of volatile organic compounds (VOCs). Therefore novel oxidation tests for the simultaneous abatement of propylene and particulate matter in a stream containing 5 vol.% of water were carried out. Characterization techniques like X-ray powder diffraction, $H_2$ temperature-programmed reduction, soot temperature-programmed reduction, $N_2$ physisorption at -196 °C, field emission scanning electron microscopy and X-ray photoelectron spectroscopy were utilized for the study of the physico-chemical properties of the powders.

# Experimental

## Catalysts Preparation

Pure manganese oxide ($Mn_2O_3$) was prepared by means of a sol-gel synthesis technique. Additionally, three other $Mn_2O_3$ samples ($MnCu_{15}$, $MnFe_{15}$ and $MnCu_{7.5}Fe_{7.5}$) were doped with transition metals (Cu and/or Fe) using the same preparation procedure. The doping of the samples was carried out assuring a transition metal(s) nominal content of 15 at.% during the synthesis, and the balance in manganese.

During the syntheses the following precursor(s) manganese (II) nitrate tetrahydrate, copper (II) nitrate trihydrate and iron (III) nitrate nonahydrate (Sigma-Aldrich), was/were dissolved in Milli-Q water (*ca.* 50 mL) along with citric acid monohydrate (Sigma-Aldrich). The total concentration of the nitrate(s) solution was of 0.2 M, while the citric acid was added maintaining a 1:1 molar ratio with the nitrate(s). Afterwards, the mixture was magnetically stirred at r.t. until the complete dissolution was achieved. The pH of this solution was raised until pH=5 by adding dropwise ammonium hydroxide (Sigma-Aldrich). Subsequently, the solution was gradually heated until 60 °C by means of a water bath (*ca.* 1 °C $min^{-1}$). Isothermal conditions were maintained for a period of 2 h, during which colloidal particles appeared in the solution and then aggregated. The solid formed was then extracted from the suspension through vacuum filtration and any remaining precursor was eliminated washing with water. After drying the sample at 60 °C overnight, it was calcined in the oven from r.t. until 550 °C (ramp: 5 °C $min^{-1}$) for 2 h.

The stability of the catalytic performance of the samples most active in soot oxidation was investigated. Therefore, the samples $Mn_2O_3$ and the $MnCu_{7.5}Fe_{7.5}$, were calcined at 750 °C for 4 h (10 °C $min^{-1}$).

## Catalysts Characterization

The specific surface area (SSA), the total pore volume ($V_p$) and the average pore diameter ($D_p$) were measured by means of a $N_2$ physisorption procedure at -196 °C in a Micromeritics Tristar II 3020. Prior to the analysis, the powder samples were subject to a degassing pretreatment at 200 °C for 2 h in order to eliminate any adventitious atmospheric pollutants and moisture. The specific surface area was calculated through the Brunauer, Emmett and Teller method (BET). On the other hand, the total pore volume and the average pore diameter were estimated by means of the Barrett-Joyner-Halenda method (BJH).

The morphologies of the catalysts were observed by means of a field emission scanning electronic microscope (FESEM) Zeiss Merlin, Gemini-II column using the following operative conditions: working distance 2.3-2.9 mm, extra high tension 3 kV and probe intensity of 100 pA.

The X-ray diffraction patterns of the powders were measured by means of an X'Pert Philips PW3040 diffractometer using Cu $K_\alpha$ radiation (2θ range = 20-80°, step = 0.05° 2θ, timer per step =0.02 s). The patterns obtained were indexed according to the Powder Data File Database (PDF 2000, International Centre of Diffraction Data, Pennsylvania). The average size of the powder crystallites was calculated using the Scherrer formula, $D=0.9\ (\lambda / b \cos\theta)$, where λ: wavelength of Cu $K_\alpha$ radiation, b: full width and half maximum (FWHM) in radians, 0.9: shape factor for spherical particles and θ: peak diffraction angle.

The temperature-programmed reduction with $H_2$ ($H_2$-TPR) were carried out in a ThermoQuest TPD/R/O 1100 analyzer, equipped with a thermal conductivity detector (TCD). Prior to the $H_2$-TPR analysis, the powder sample (20 mg) was pretreated inside the tubular reactor at 500 °C under a He flow (40 mL $min^{-1}$). The $H_2$-TPR was performed by feeding 5 vol.% $H_2$ in Ar (20 mL $min^{-1}$) in the reactor and raising the temperature from r.t. to 800 °C (5 °C $min^{-1}$).

The reducibility of the catalyst by soot was investigated performing a soot-TPR analysis. The reduction was carried out in a quartz U-tube reactor (ID = 4mm), hosting a fixed-bed containing the catalyst (45 mg), soot (5 mg) and silica (150 mg) in "tight contact" and heated by a PID-controlled furnace. In order to assure an intimate soot-catalyst contact, the bed mixture was ground in a ball-milling apparatus at 250 rpm for 15 min. Prior to the analysis, a pretreatment was performed by feeding $N_2$ (100 mL $min^{-1}$) at 100 °C for 30 min. Afterwards, the soot-TPR was conducted under the same flow of $N_2$ and raising the temperature until 700 °C (5 °C $min^{-1}$). The outlet concentrations of CO and $CO_2$ were measured using NDIR analyzers.

The XPS (X-ray photoelectron spectroscopy) technique was performed in an XPS PHI 5000 Versa probe apparatus: band-pass energy = 187.85 eV, take off angle = 45° and diameter X-ray spot size: 100 μm. The curves were fitted by means of the Multipack 9.0 software.

## Catalytic Activity Tests

The catalytic activity of the powders was evaluated in a temperature-programmed oxidation setup. The screening was carried out in a micro-reactor comprising a fixed-bed in a quartz U-tube with inner diameter = 4 mm and heated by and electric PID-controlled furnace. During the soot oxidation tests, the bed mix contained 45 mg of catalyst, 5 mg of carbon soot and 150 mg of $SiO_2$ that were gently mixed with a spatula for 3 min, and thus assuring "loose contact" soot-catalyst condition. Before the catalytic test, the powder-mix was pretreated in 100 mL $min^{-1}$ of $N_2$ at 100 °C for 30 min. Afterwards, the catalytic test was performed under a gaseous flow mix containing 50 vol.% of $N_2$ and 50 vol.% of air was fed in the reactor (100 mL $min^{-1}$). As well, the temperature was increased until 700 °C (5 °C $min^{-1}$). Subsequently, the concentrations of CO and $CO_2$ produced during the oxidation of soot were measured by means of NDIR analyzers.

On the other hand, the catalytic activity in the oxidation of volatile organic compounds was investigated using propylene as probe molecule. During these tests, the fixed-bed contained 100 mg of catalyst (pellets of 212-300 µm). Prior to the catalytic tests, a degassing pretreatment in $N_2$ (100 mL $min^{-1}$) was performed for 1 h at 150 °C, in order to remove any atmospheric pollutant. Afterwards, the catalytic test was carried out by feeding a gaseous mixture (100 mL $min^{-1}$) containing 500 ppm of $C_3H_6$, 10 vol.% of $O_2$ and the balance in $N_2$. The temperature was raised (5 °C $min^{-1}$) from room temperature until the total conversion of the propylene fed was achieved. The reproducibility of the catalytic performance of the most active catalyst was studied by means of two consecutive catalytic tests. Additionally, the catalytic stability of the aforementioned catalyst was investigated in a long-term (7 h) test and switching the operative temperature every hour.

The simultaneous VOC-soot catalytic oxidation test was conducted using propylene ($C_3H_6$) as a VOC probe molecule. The test was performed in a fixed-bed reactor loaded with soot in "loose" contact conditions. The reactive gaseous mix fed to the reactor (100 mL $min^{-1}$) contained 500 ppm di $C_3H_6$, 10 vol.% of $O_2$ and the balance in $N_2$. During the test the temperature was raised at a constant rate (3 °C $min^{-1}$) until 700 °C. The 5 vol.% content of water in the reactor-inlet was assured by saturating the gaseous stream in an evaporator system containing water.

# Results and Discussion

## Material Textural Properties

The morphologies of the samples prepared via sol-gel synthesis are summarized in Figure 1. In agreement with previous studies, the micrographs, as well as the calculated average pore diameters included in Table 1 (*vide infra*) evidence that the prepared samples are characterized by mesoporous structures [14]. Interestingly, the morphology of the oxides consists in a "flake-like" arrangement composed of an external shell and a void interior that resembles a honeycomb structure. On the other hand, the BET specific surface areas calculated after performing the $N_2$ physisorption are included in the Table 1. The values obtained evidence that the BET SSA of the metal-doped samples slightly decreased, compared to the one of the parent $Mn_2O_3$ oxide. Likewise, the volume of the pores ($V_P$=0.09-0.11 $cm^3$ $g^{-1}$) evidences a slightly decreasing trend when the foreign metals are inserted in the structure of the manganese oxide.

**FIGURE 1** Morphologies of the prepared catalysts as observed in FESEM.

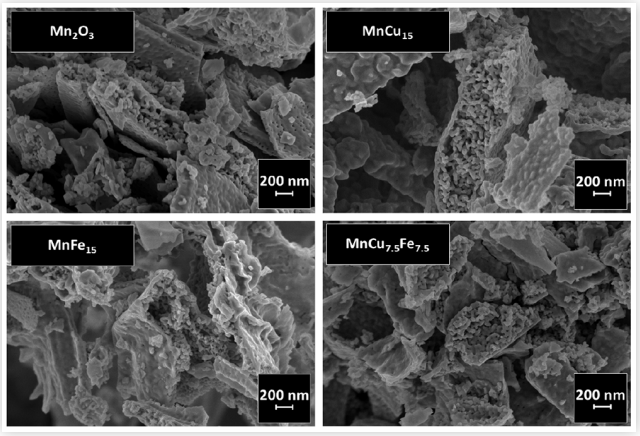


Interestingly, the size of the crystallites calculated by means of the Scherrer formula decreased when iron and copper were inserted in the structure separately. However, when both metals were present in the system, the size of the crystallite remained unchanged.

The diffraction patterns obtained during the XRD analyses are summarized in Figure 2a. As a general behavior, the profiles obtained correspond to the diffraction of the manganese oxide (II) cubic crystal system (reference code 01-078-0390). These results suggest that the formation of other

**TABLE 1** Structural and textural properties of the fresh and aged oxides, as calculated from $N_2$ physisorption at -196 °C and X-ray diffraction analyses.

| Catalyst | $S_{BET}$[a] [$m^2$ $g^{-1}$] | $V_P$[b] [$cm^3$ $g^{-1}$] | $D_P$[c] [nm] | Crystallite Size[d] [nm] | *a* [nm] |
|---|---|---|---|---|---|
| $Mn_2O_3$ | 13 | 0.11 | 32 | 73 | 0.945 |
| $MnCu_{7.5}Fe_{7.5}$ | 12 | 0.11 | 37 | 73 | 0.944 |
| $MnCu_{15}$ | 12 | 0.10 | 33 | 56 | 0.946 |
| $MnFe_{15}$ | 10 | 0.09 | 34 | 69 | 0.948 |
| Aged-$Mn_2O_3$ | 6 | 0.02 | 12 | 108 | 0.947 |
| Aged-$MnCu_{7.5}Fe_{7.5}$ | 6 | 0.02 | 15 | 112 | 0.945 |

[a] Specific surface area calculated through the BET method

[b] Cumulative volume of pores calculated according to the BJH method

[c] Average pore diameter calculated according to the BJH method

[d] Crystallite size calculated through the Scherrer formula

[e] Cell parameter

**FIGURE 2** XRD diffraction patterns of the prepared catalysts (Section A) and magnification of the most intense peak signal (Section B).

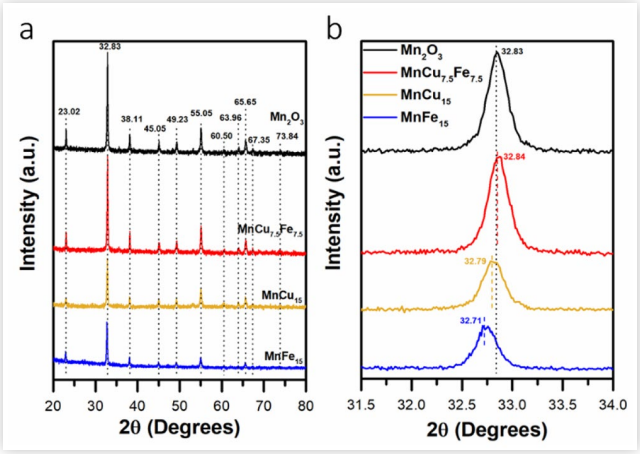


oxides (like CuO or $Fe_2O_3$) did not take place, and thus that the metals were well-incorporated in the crystalline structure. On the other hand, the magnifications of the diffraction patterns are showed in the Figure 2b. It was observed that the single insertion of copper or iron translated the most intense peak from 32.83° to lower 2θ values (32.79° and 32.71° respectively). Consistently, these results evidence that an expansion of the $Mn_2O_3$ crystalline structure occurred. This can be ascribed to the presence of Cu and Fe that induce strain in the crystalline system due to their bigger ionic radii [$r_{ionCu}$ $Cu^{+}/Cu^{2+}$ = 0.077/0.073 nm with coordination number (CN) =6, while $r_{ionFe}$ $Fe^{2+}/Fe^{3+}$ = 0.061/0.055 nm with CN=6], compared to that of Mn ions [$r_{ionMn}$ $Mn^{3+}/Mn^{4+}$ = 0.058/0.053 nm with CN=6] [15].

Additionally, the variation of the physico-chemical properties of the $Mn_2O_3$ and the ternary catalyst are reported in Table 1. It is evidenced that the BET surface area decreased in both cases and reached a value of *ca.* 6 $m^2 g^{-1}$. As well, the pore diameter and the pore volume showed a marked decrease. These changes occurred probably due to the sintering of the particles that may take place at the severe thermal aging conditions (750 °C, 4 h). Moreover, it was observed that the crystalline properties changed as well, and showed to increase in both cases (namely, size of crystallites and cell parameter).

## $H_2$ Temperature-Programmed Reduction

The $H_2$-uptake profiles of the prepared oxides as a function of the temperature are included in the Figure 3. The reduction profile of the sample $Mn_2O_3$ (black line) evidences two reduction peaks centered at 352 °C and 486 °C. The former is ascribed to the following reduction step $Mn_2O_3 \rightarrow Mn_3O_4$, while the latter corresponds to the reduction of $Mn_3O_4 \rightarrow MnO$ [14, 16, 17]. Interestingly, the deconvolution of the $H_2$ consumption profile is equivalent to 6.99 mmol $g^{-1}$ (see Table 2). However, the theoretical consumptions are equal to 6.33 mmol $g^{-1}$ for the $Mn_2O_3 \rightarrow MnO$ reduction step, and of 11.50 mmol $g^{-1}$ for the $MnO_2 \rightarrow MnO$. This indicates that $Mn^{4+}$ cations are present in the sample and thus increase slightly the $H_2$ consumption compared to the theoretical amount.

**FIGURE 3** Reducibility profiles of the prepared catalysts observed during $H_2$-TPR analyses.

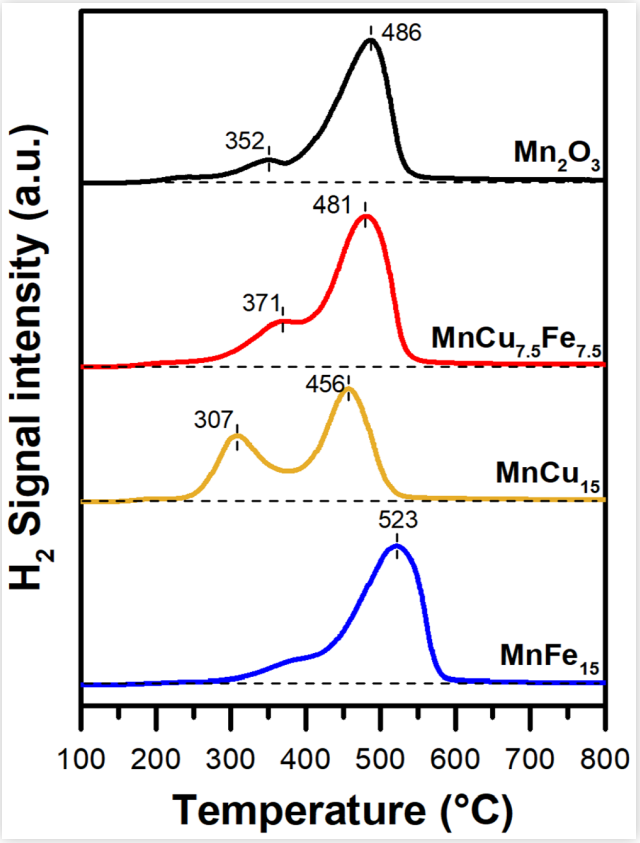


**TABLE 2** Consumption of hydrogen of the prepared catalyst during the $H_2$-TPR.

| Catalyst | $H_2$ uptake [mmol $g_{cat}^{-1}$] |
|---|---|
| $Mn_2O_3$ | 6.99 |
| $MnCu_{15}$ | 7.22 |
| $MnFe_{15}$ | 8.25 |
| $MnCu_{7.5}Fe_{7.5}$ | 8.48 |

The signal corresponding to the reduction of the Cu doped sample, thus the $MnCu_{15}$ (magenta line), shows two intense peaks with maximum signal at 307 °C and 456 °C. This evidences that the formation of a Mn-O-Cu mixed lattice enhances the reduction of the parent oxide ($Mn_2O_3$) at lower temperatures. Since the reduction of copper species may take place at *ca.* 210-300 °C [18], the signal occurring at 307 °C was assigned to the parallel reduction of $Cu^{x+}$ and $Mn^{3+}$ species. While the signal located at higher temperature was attributed to the further reduction of $Mn^{3+}$ cations. The $MnCu_{15}$ thus evidenced to be the most reducible sample at lower temperatures, compared to the other catalysts. This evidences a positive role of the copper species that are doping the parent oxide.

On the other hand, during the $H_2$-TPR of the $MnFe_{15}$ (blue line) and intense signal is observed at 523 °C with a side

peak that starts at lower temperature (*ca.* 300 °C). The occurrence of this signal at a higher temperature, compared to the parent oxide, indicates that the $Fe^{x+}$ cations introduced in the system enhanced the formation of a chemical structure more resistant to reduction. Therefore, and according to the literature, the reduction taking place at low temperatures (below 530 °C) can be assigned to the change of oxidation state (from 3+ to 2+) of Mn and Cu species. Instead, the signal occurring at higher temperature is attributed to the reduction step $Fe^{2+} \rightarrow Fe$ [19, 20].

The reduction profile of the $MnCu_{7.5}Fe_{7.5}$ (red line) is characterized as well by two intense signal occurring at 371 °C and 481 °C. The behavior is comparable to that of the parent $Mn_2O_3$. However, the differences are the increased $H_2$ consumption taking place below 400 °C and the slight shifting of the signal maxima observed. Consistently, the reduction profile seems an intermediate behavior between the $MnFe_{15}$ and the $MnCu_{15}$. Consistently, the signal occurred at low temperature was attributed to the reduction step $Cu^{x+} \rightarrow Cu^0$ and the initial reduction of $Mn^{3+}$ and $Fe^{3+}$ cations. On the other hand, the signal appeared at higher temperature was assigned to the further reduction of manganese and iron cations.

## Soot Temperature-Programmed Reduction

Figure 4 summarizes the reducibility by soot of the prepared oxides in terms of $CO_2$ and CO produced during the soot-TPR. In general, a low-intensity $CO_2$ signal occurs in the 150 °C - 300 °C temperature range. On the other hand, the signal occurred at higher temperature is composed of a rather complex ensemble of peaks. The former signal can be assigned to the release of $CO_2$ adsorbed (presumably from the atmosphere) in basic sites of the manganese oxides [21]. Since $O_2$ is not present in the stream, the latter CO and $CO_2$ signal correspond to the oxidation of soot by means of the oxygen species present in the catalyst. According to the literature, the oxidation taking place in the range 350-450 °C occurs due to surface chemisorbed $O_2^-$ species, while at higher temperatures (*ca.* 450-550°C) the oxidation of soot occurs by means of more electronegative oxygen species like $O_2^{2-}$ or $O^-$ [22, 23]. The highest oxidation rate takes place at T>550°C, accordingly, it is attributed to the reduction of the species in the bulk, *i.e.* by means of the lattice oxygen present in the bulk. The amount of soot oxidized during the soot-TPR analyses, according to the temperature range, is included in Table 3. Considering the aforementioned discussion, the amount of soot burnt between 300 °C and 550 °C is related to the oxidation due to the active surface-chemisorbed oxygen species. Therefore, these values are indicative of the ability of the catalysts to initiate the catalytic conversion of soot at low temperature. Whereas the soot oxidizing over 550 °C is related to the reducibility of the bulk catalyst. Consistently, it can be stated that the reducibility of the prepared manganese oxides by soot increases with the insertion of a foreign metal (Cu and/or Fe) in the structure, as follows: $Mn_2O_3 < MnCu_{7.5}Fe_{7.5} < MnFe_{15} < MnCu_{15}$.

**FIGURE 4** Reducibility of the synthesized catalysts by soot as observed in the soot-TPR investigations.

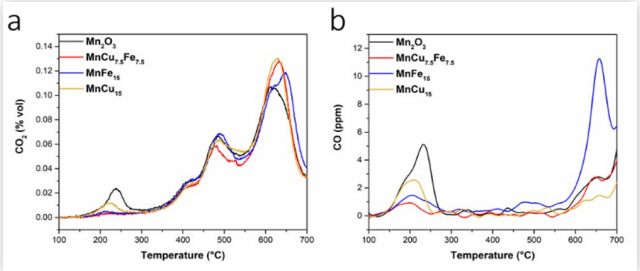


**TABLE 3** Amounts of soot burnt during the soot-TPR analyses.

| Catalyst | Soot burnt $^{300\text{-}550\ °C}$ [mg] | Soot burnt $^{550\text{-}700\ °C}$ [mg] |
|---|---|---|
| $Mn_2O_3$ | 0.73 | 1.09 |
| $MnCu_{15}$ | 0.71 | 1.18 |
| $MnFe_{15}$ | 0.81 | 1.14 |
| $MnCu_{7.5}Fe_{7.5}$ | 0.72 | 1.12 |

## X-Ray Photoelectron Spectroscopy

A summary of the XP spectra obtained during the XPS analysis in shown in Figure 5. Specifically, **Section a,** evidences the spectra obtained in the Mn *2p* core level and their corresponding deconvolution. The signal corresponding to the $2p_{3/2}$ level is observed in the 637.5-648.0 eV binding energy (BE) range. Instead, the spectra related to the $2p_{1/2}$ level is observed in the 648.0-658.0 eV range. Several works in the literature have reported that an estimation of the amount of the various manganese species (namely, $Mn^{4+}$, $Mn^{3+}$ and $Mn^{2+}$) can be calculated by means of the deconvolution of the $2p_{3/2}$ level signal [14, 16, 24]. Accordingly, the signal peaks observed were centered between 640.7-640.9 eV for the $Mn^{2+}$, between 641.8-642.1 eV for the $Mn^{3+}$ and between 644.1-644.8 for the $Mn^{4+}$ specie. The relative amounts of the $Mn^{x+}$ species obtained after the deconvolution of the spectra is reported in Figure S1**.** It is evident that the insertion of Fe and/or Cu in the structure of the parent $Mn_2O_3$ increased the amount of manganese species with higher oxidation state ($Mn^{4+}$) present in the catalyst. This behavior evidences the role of Fe and Cu in the comparison of more oxidized Mn species. Particularly, it was observed that the catalyst with the highest content of Cu (namely, the $MnCu_{15}$) contained a prominent content of Mn with lower oxidation state, thus $Mn^{2+}$ species.

The XP spectra observed in the O 1*s* core level and their deconvolution are summarized in Figure 5b. As a general behavior, the spectra are composed of two peaks centered at different binding energies. Consistently, the peaks can be assigned to different oxygen species, namely surface chemisorbed oxygen ($O_\alpha$-species) and lattice ($O_\beta$) oxygen (thus the $O^{2-}$ species bonded to the metals). Therefore, the signal centered at lower BE (between 529.4-529.9 eV) were assigned to nucleophilic $O_\beta$ bonded to Mn, Fe or Cu [25]. Instead, the signal occurring at higher BE values (between 531.2-531.5 eV)

**FIGURE 5** Mn (2*p*), O (1*s*), Fe (2*p*) and Cu (2*p*) core level spectra obtained during the XPS analyses.

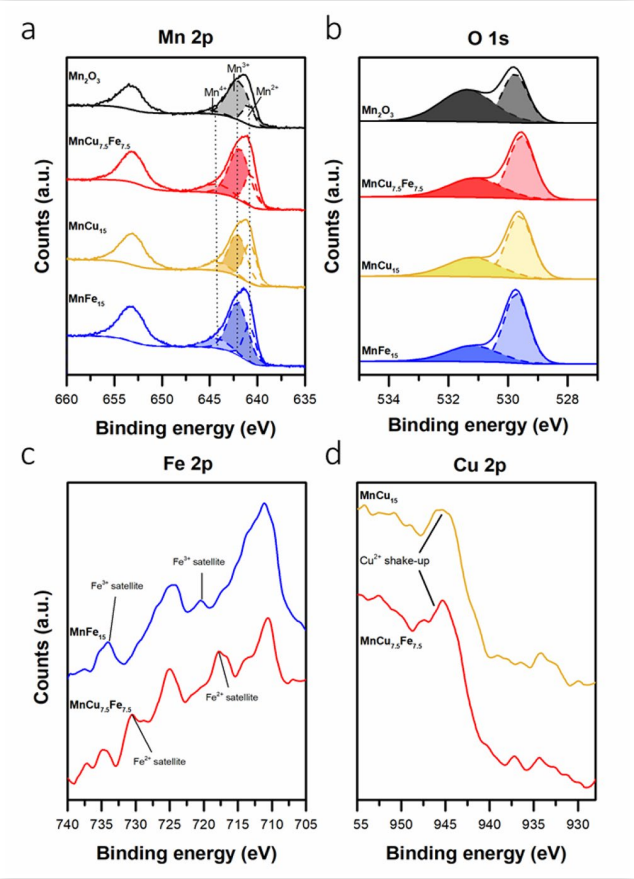


was attributed to electrophilic $O_\alpha$-species like $O_2^-$, $O^-$ and to OH groups [16, 26]. As it is evidenced in Figure S2, the parent oxide ($Mn_2O_3$) showed the highest content of $O_\alpha$-species, thus assuring the highest $O_\alpha/O_\beta$ ratio (*ca.* 1.33). On the other hand, the catalysts containing $Cu^{x+}$ species (*i.e.* the $MnCu_{7.5}Fe_{7.5}$ and the $MnCu_{15}$) showed similar $O_\alpha/O_\beta$ ratios (0.67 and 0.62 respectively), whereas the lowest value was observed in the mixed oxide containing Fe (*ca.* 0.45).

The XP spectra observed in Figure 5c correspond to the signal observed in the Fe 2*p* core level. The signal observed between 707.0-717.0 eV corresponds to the $2p_{3/2}$ level, whereas the signal observed in the BE range between 723.0-728.8 eV is attributed to the $2p_{1/2}$ level. According to the literature, the presence of the different Fe species (namely, $Fe^{2+}$ and $Fe^{3+}$) can be assessed by observing the aforementioned signal and the eventual satellites related to them [24, 27]. Observing the spectra of the $MnCu_{7.5}Fe_{7.5}$ and the $MnFe_{15}$, intense peaks occurred at 710.7 and 711.1 eV respectively. As well, satellites related to the $Fe^{3+}$ specie can be observed (mostly in the $MnFe_{15}$ catalyst), thus evidencing the presence of an important amount of $Fe^{3+}$ in both catalysts. On the other hand, the spectrum of the ternary $MnCu_{7.5}Fe_{7.5}$ evidenced satellites at *ca.* 716.9 and 730.6 eV related to the presence of the specie $Fe^{2+}$, thus suggesting its presence in the ternary catalyst. Particularly, the occurrence of the reduced $Fe^{2+}$ coincides with an elevated amount of the oxidized $Mn^{4+}$ specie in the ternary catalyst (*vide supra*). This may suggest that substituting $Mn^{3+}$ species in the lattice with Cu and Fe simultaneously can enhance the formation of the reduced $Fe^{2+}$ specie in the crystalline structure.

The signal observed in the Figure 5d corresponds to the XP spectra retrieved in the Cu 2*p* core level. According to the literature, the signal appeared at *ca.* 930.0-937.0 eV corresponds to the $2p_{3/2}$ level. This BE region can be utilized for the identification of the oxidation state of the $Cu^{x+}$ species and, eventually, for the quantification of their relative abundances in the sample [7, 28, 29, 30]. Though the low intensity signal does not allow a precise quantification of the different $Cu^{x+}$ species in the mixed oxides, the shake-ups corresponding to $Cu^{2+}$ observed in both spectra suggest the presence of these species in the catalysts, *i.e.* the presence of Cu with oxidation state +2.

## Catalytic Activity

**Soot Oxidation** The experimental data obtained during the conversion of soot in function of the temperature reached by the prepared catalysts in "loose" contact conditions is evidenced in Figure 6. It can be observed that the prepared catalysts performed the oxidation of soot at temperatures lower than those required for the thermal oxidation, *i.e.* the non-catalyzed reaction. The amount of soot converted to $CO_x$ during the catalytic and non-catalytic screenings are included in the Figure 6 **(sections a and b)**. Considering the uncatalyzed reaction (green dotted line), a highly unselective oxidation takes place. In other words, the combustion of carbonaceous matter lead to the formation of a relatively elevated amount of CO in absence of a catalyst. Consistently, the minimal outflowing amount of CO during the catalyzed reactions demonstrates the high selectivity of the prepared catalysts towards the complete oxidation of the particulate matter.

As a general behavior, the catalyzed tests evidenced two different low-temperature signals corresponding to outflowing $CO_2$ at ca. 200 °C and 340 °C. The former was assigned to $CO_2$ species adsorbed over the catalyst's basic sites (as discussed in the soot-TPR section, *vide supra*) and thus, was not considered during the calculation of the soot conversion. On the other hand, the latter signal was attributed to the oxidation of soot particles that are in "tight" contact with the catalysts. Interestingly, since the catalytic beds were assembled through a standard "loose contact" preparation, this signal was unexpected. This evidences that a physico-chemical property of the catalysts may have enhanced the occurrence of "tight" contact points between the soot particles and the catalyst and therefore the soot oxidation at lower temperature. In accordance with the literature, a well-defined nanostructure favors the occurrence of low-temperature catalytic activity for soot oxidation, due to increased number of catalyst-soot contact points [12, 31]. The catalytic performances of the catalysts in soot oxidation in terms of $T_{X\%}$ and reaction rate is included in Table 4. In general, when considering the temperatures for converting 50% of the soot, *i.e.* the $T_{50\%}$, the $Mn_2O_3$ and the mixed $MnCu_{7.5}Fe_{7.5}$ evidenced fairly equivalent performances, and the best, observed among the catalysts prepared in this work. On the other hand, the $MnCu_{15}$ evidenced the worst

**FIGURE 6** Amount of $CO_2$ (Section A) and CO (Section B) produced and conversion (%) curves (Section C) as a function of the temperature observed in the catalytic oxidation of soot, performed in "loose" contact conditions over the prepared catalysts.

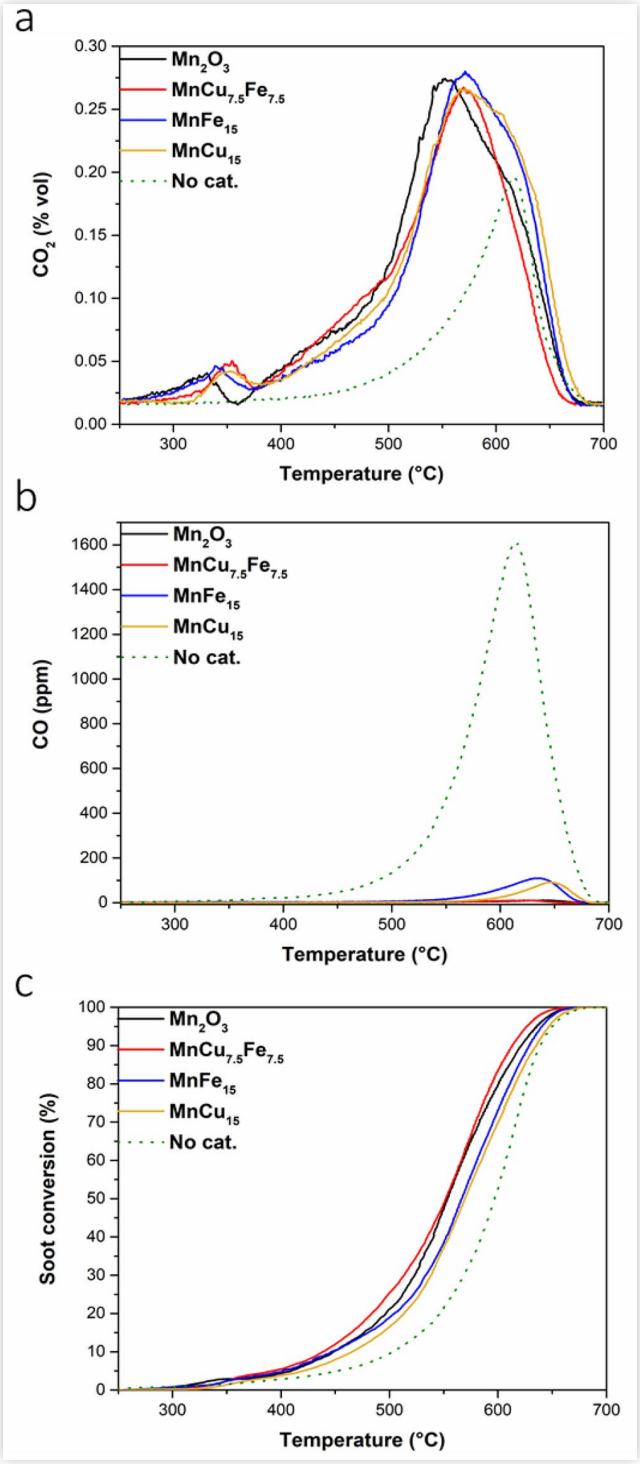


catalytic performance in terms of both $T_{X\%}$ and soot oxidation reaction rate. In this sense, a decreasing pattern for the catalytic performance can be suggested, as follows: $Mn_2O_3 \approx MnCu_{7.5}Fe_{7.5} > MnFe_{15} > MnCu_{15}$. Except for the catalyst $MnFe_{15}$, the suggested pattern is in line with the relative amount of chemisorbed oxygen species that was estimated through the XPS analyses (*vide supra*).

**TABLE 4** Performance of the prepared catalysts in the oxidation of soot in terms of $T_{10\%}$, $T_{50\%}$, $T_{90\%}$ and reaction rate at 415 °C

| Catalyst | $T_{10\%}$ [°C] | $T_{50\%}$ [°C] | $T_{90\%}$ [°C] | $r_{soot}$[a] [mmol $h^{-1}$ $g^{-1}$] |
|---|---|---|---|---|
| $Mn_2O_3$ | 449 | 553 | 622 | 2.10 |
| $MnCu_{15}$ | 466 | 570 | 636 | 1.42 |
| $MnFe_{15}$ | 447 | 567 | 630 | 1.54 |
| $MnCu_{7.5}Fe_{7.5}$ | 440 | 552 | 613 | 1.91 |

[a] calculated at 415 °C

The literature has evidenced that the oxidative activity of various oxide catalysts occurs through superficial cycles of oxidation-reduction, in which the structural oxygen of the catalyst takes part, *i.e.* the Mars-van Krevelen mechanism [7, 32] . In this type of mechanism an elevated oxygen mobility is a fundamental parameter, in other words an enhanced reducibility, as well as catalyst structural defects should improve the oxidative performance [7, 14, 18]. However, the catalytic activity trend observed in this work cannot be attributed to the reducibility improvement observed after doping the manganese oxide with Cu and/or Fe. Interestingly, the calculated soot oxidation reaction rates seem related to the $Mn^{3+}/Mn^{2+}$ ratio that were obtained by means of the deconvolution of the Mn 2*p* core level spectra. As observed in Figure S3, the soot oxidation reaction rate follows a decreasing trend when the relative amount of reduced $Mn^{2+}$ species is higher. As observed, the trend was assessed by means of a linear fitting (solid red line), while the dashed red lines represent the 95% confidence bands. Considering the aforementioned discussion, this finding suggests that the reduced $Mn^{2+}$ cations may not be taking part in the redox cycle and thus could be diminishing the oxidative performance of the catalysts. Consistently, in a previous investigation it was observed how elevated amounts of $Mn^{2+}$ species decreased the oxidative performance of oxide catalysts [18]. Therefore, this suggests that the $Mn^{2+}$ cations present in the catalyst do not actively take part in the reactive redox pathway, under the utilized reactive environment.

Additionally, the catalytic performance of the most promising catalysts, thus the $Mn_2O_3$ and the $MnCu_{7.5}Fe_{7.5}$, was studied under "tight" contact soot-catalyst conditions (see Figure 7). The solid lines observed in the graphs correspond to the test carried out in "loose" contact, whereas the dashed lines correspond to the data obtained during the "tight" contact tests. As a whole, the signal corresponding to the $CO_2$ produced during the catalytic tests (see Figure 7a) generally translated to lower temperature values ca. 400 °C.

Similarly, the CO (Figure 7b) signal occurred at lower temperatures and with a further reduced intensity, compared to the one of the "loose" contact tests. Consistently, the elevated conversions observed in "tight" contact conditions (see Figure 7c) evidenced the catalytic superiority of the prepared $Mn_2O_3$ ($T_{50\%}$ = 420 °C) compared to the doped oxide $MnCu_{7.5}Fe_{7.5}$ ($T_{50\%}$ = 455 °C). These results evidence how maximizing the contact points between the particulate matter and the catalysts highly enhanced the catalytic performance. It can be observed that the reaction was initiated at the lowest temperatures in the case of the $Mn_2O_3$ catalyst, compared to

**FIGURE 7** Amount of $CO_2$ (Section A) and CO (Section B) produced and conversion (%) curves (Section C) as a function of the temperature observed in the catalytic oxidation of soot, performed in "tight" contact conditions over the $Mn_2O_3$ and the $MnCu_{7.5}Fe_{7.5}$ catalysts.

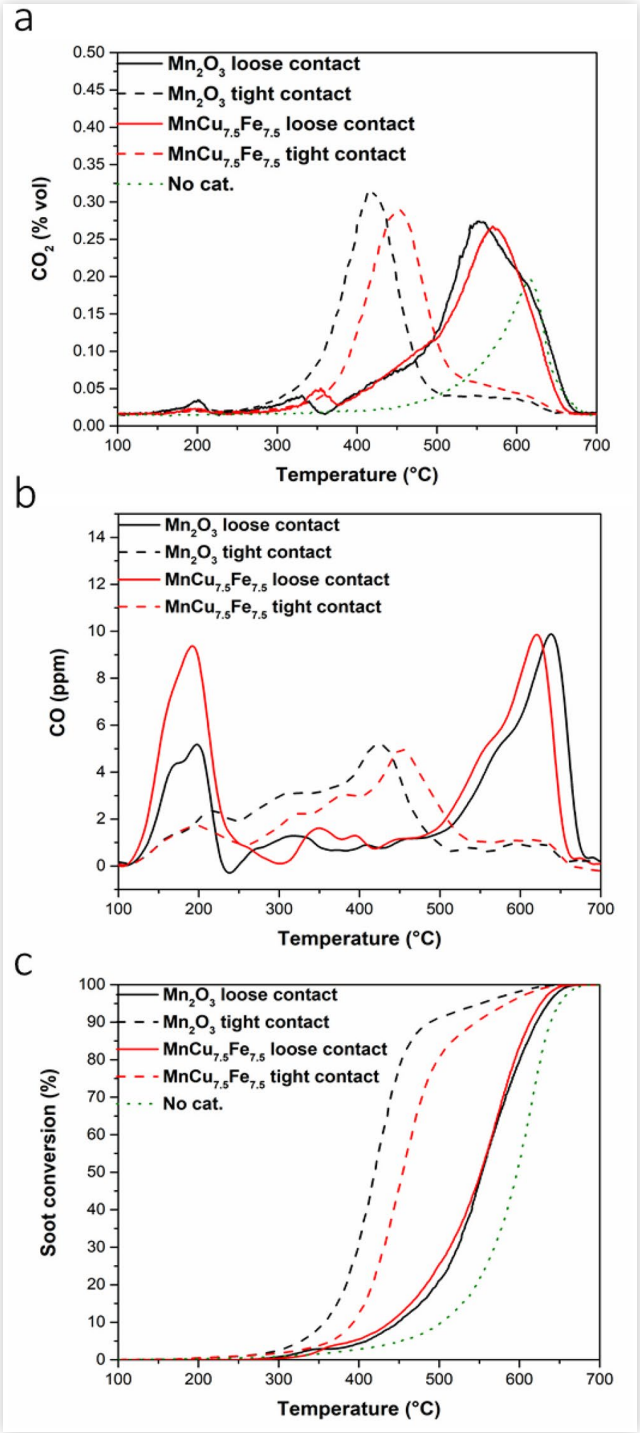


those of the $MnCu_{7.5}Fe_{7.5}$. This coincides with the catalysts ability to start the soot oxidation reaction by means of the surface-chemisorbed oxygen species, which in turn is in accordance with the $O_\alpha/O_\beta$ trend observed in the XPS analyses (*vide supra*). Therefore, these results evidence the important role of the surface-chemisorbed oxygen species in low-temperature catalytic soot oxidation.

Additionally, the stability of the catalytic activity of the parent $Mn_2O_3$ and the ternary oxide was assessed. The study was performed using the catalysts previously aged in a furnace (see section 2.1). The results obtained in terms of produced $CO_2$, CO and soot conversion are included in Figure S4. The observed dashed lines correspond to the data obtained during the catalytic testing of the aged catalysts. Observing the $CO_2$ produced during the testing of the aged catalysts, a side peak at ca. 615 °C can be noticed. Moreover, the formation of CO became noticeable as well (see Figure S4bd). These signals are in correspondence with the non-catalytic thermal conversion of soot, and thus suggest a slight deactivation of both catalysts at low temperatures. The worsening of the performance was attributed to the probable sintering of the catalyst during the ageing treatment. This procedure affected the surface areas available, by reducing them from ca. 13 $m^2\ g^{-1}$ to 6 $m^2\ g^{-1}$ in both cases (see Table 1). Moreover, this variation may have induced a variation of the monolithic morphology of the catalysts or the reduction of surface-chemisorbed species which demonstrated to be beneficial in the soot oxidation process.

The catalytic performance of the prepared $Mn_2O_3$ was assessed as well when a humidity content of 5 vol.% is present in the stream. The results obtained during this test are summarized in Figure 8. Remarkably, the $CO_2$ profiles retrieved during both oxidation tests are rather similar (see Figure 8a). However, the side peak occurring at high temperature (*ca.* 615 °C) showed a slight enhancement when water was present in the stream. Likewise, a higher amount of CO (see Figure 8b), compared to the test performed in "dry" condition, was observed in the same temperature range, suggesting that non-catalytic thermal oxidation may appear in presence of water. Interestingly, these findings evidence that the presence of water is mostly negligible during the oxidation of soot oxidation the $Mn_2O_3$ and thus, at some extent, the resistance of the oxidative activity of the catalyst to water vapors present in the gaseous stream. These results coincide with other works reported in the literature [33, 34].

**Propylene Oxidation** The conversion of propylene by the prepared catalysts as a function of the temperature is shown in Figure 9. As well, these performances are summarized in Table 5 in terms of propylene reaction rate and $T_{10\%}$, $T_{50\%}$ $T_{90\%}$.

The aforementioned temperatures observed for the doped catalysts during the VOC elimination tests did not evidence a significant variation compared to those of the parent $Mn_2O_3$. However, it was observed that the calculated specific reaction rates (*i.e.* the catalytic oxidation of propylene) increased when the $Mn_2O_3$ was doped with Cu and/or Fe. Interestingly, the highest reaction rate obtained corresponds to the catalyst that evidenced (during the $H_2$-TPR) the best reducibility at low temperatures, thus the $MnCu_{15}$. These results suggest that the insertion of the foreign metals (Cu and/or Fe) in the structure of $Mn_2O_3$ (as demonstrated in the XRD analyses) can improve its catalytic performance in the oxidation of VOCs. According to the literature, the preparation of mixed manganese-oxides using transition metals may enhance the presence of oxygen vacancies, and thus the formation of a defective oxide

**FIGURE 8** Amount of $CO_2$ (Section A) and CO (Section B) produced and conversion (%) curves (Section C) as a function of the temperature observed in the catalytic oxidation of soot, performed in "loose" contact conditions over the $Mn_2O_3$ catalyst in presence of 5 vol.% of water.

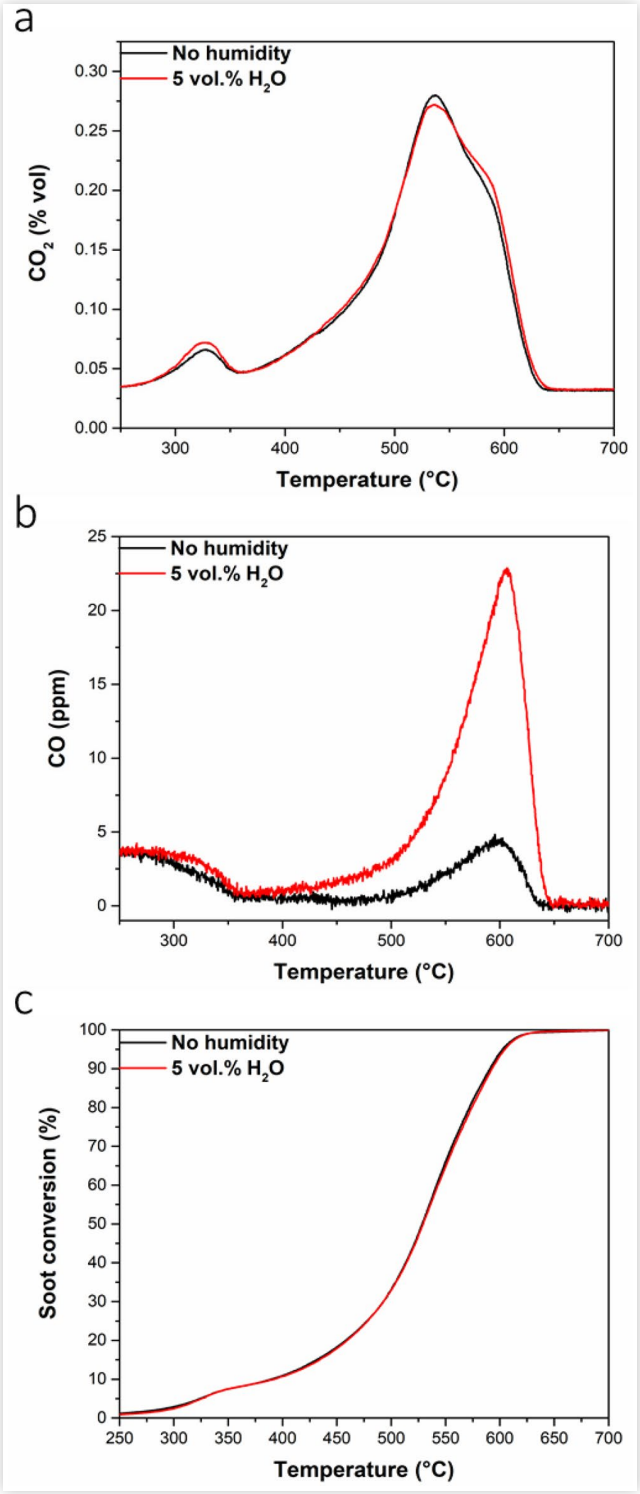


structure [35, 36]. Consistently, these parameters are thought to be the key parameters for the enhanced catalytic activity in propylene oxidation of the doped manganese oxides studied in this work. Finally, two consecutive oxidative tests were performed using the most active catalyst, thus the $MnCu_{15}$, in order to verify the reproducibility of the overall catalytic performance. As observed in Figure S5, no significant variation in the catalytic performance can be noticed between the first and the second catalytic tests.

**FIGURE 9** Catalytic conversion (%) of propylene as a function of the temperature over the prepared catalysts.

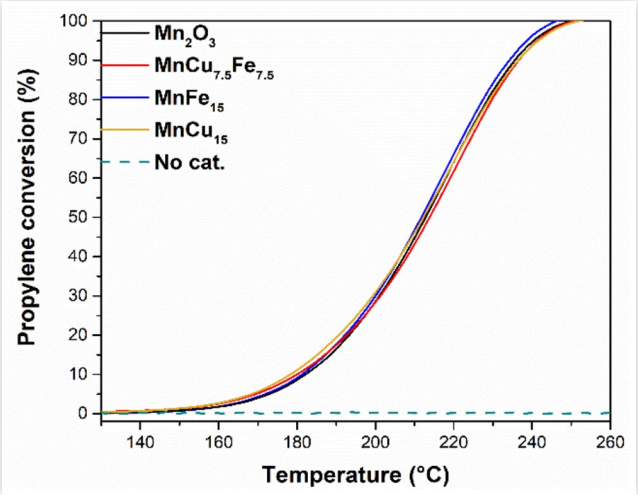


**TABLE 5** Performance of the prepared catalysts in the oxidation of propylene in terms of $T_{10\%}$, $T_{50\%}$, $T_{90\%}$ and reaction rate at 170 °C

| Catalyst | $T_{10\%}$ [°C] | $T_{50\%}$ [°C] | $T_{90\%}$ [°C] | $r_{pr}$[a] [μmol $h^{-1}$ $m^{-2}$] |
|---|---|---|---|---|
| $Mn_2O_3$ | 182 | 213 | 236 | 3.83 |
| $MnCu_{15}$ | 178 | 212 | 236 | 5.86 |
| $MnFe_{15}$ | 181 | 212 | 234 | 5.30 |
| $MnCu_{7.5}Fe_{7.5}$ | 180 | 214 | 237 | 5.36 |

[a] calculated at 170 °C

On the other hand, the long-term catalytic stability of the best catalyst (i.e. the $MnCu_{15}$) was studied in a time on stream (TOS) test at variable temperature conditions. Consistently, the conversion of propylene over the $MnCu_{15}$ as a time on stream at cyclic temperature conditions is summarized in Figure 10. As a whole, the performance of the catalyst at the tested temperatures did not evidence any deactivation after the 7 h on stream. As well, the catalytic conversion showed to be stable after 1 h in all the stages of the test. Therefore, the catalytic activity was demonstrated to be stable and reproducible over the time when it is subject to cyclic temperature conditions.

In order to analyze the effect of humidity in the oxidation of propylene over the $MnCu_{15}$ catalyst, further tests were performed assuring a content of 5 vol.% of $H_2O$ in the gaseous stream. A comparative summary of the results obtained during the propylene oxidation test in dry conditions and with 5 vol.% of water is included in Figure 11. Interestingly, it was observed that the overall catalytic performance of the catalyst remained mostly unchanged in spite of the humidity present in the stream. However, the conversion of propylene occurring in the low-temperature range evidenced a slight decrease when water is present in the stream. This finding suggests that water molecules

**FIGURE 10** Conversion (%) of propylene over the $MnCu_{15}$ as a function of the TOS in swinging temperature operative conditions.

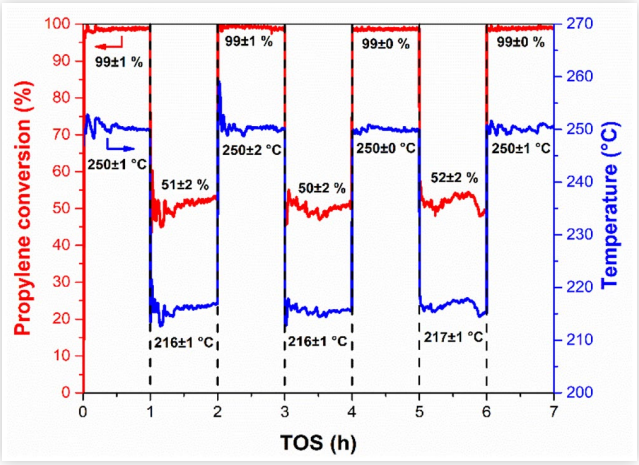


**FIGURE 11** Comparison of the catalytic conversions (%) of propylene over the $MnCu_{15}$ catalysts without humidity and in presence of 5 vol.% of $H_2O$ in the stream.

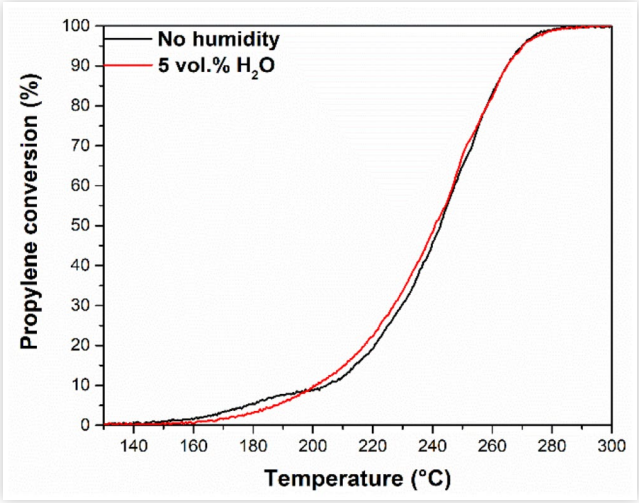


could be adsorbing onto the sites active for the oxidation. As the literature evidences, this condition can be ascribed to water molecules competitively adsorbing onto the active sites of the transition oxide, thus causing a slight worsening of the VOC oxidation [37, 38]. As a conclusion, the overall performance of the studied catalyst in the oxidation of $C_3H_6$ can be considered to remain unvaried in presence of 5 vol.% of $H_2O$.

Further analyses were performed in order to better investigate the kinetics of the propylene oxidation occurring over the $MnCu_{15}$ catalyst. Four isothermal tests (at 150, 160, 170 and 180 °C) were conducted by varying the concentration of propylene in each test between 75 ppm, 100 ppm, 200 ppm, 300 ppm and 500 ppm, while assuring a high excess of $O_2$ (*ca.* 10 vol.%), diluted in $N_2$. The operative conditions applied were analogous to those of the propylene oxidation tests. As observed in Figure S6, the oxidation rate of propylene increased in a fairly linear trend when the inlet concentration was increased and, as well, when the temperature was raised. On the other hand, the variation of the oxygen reaction rate was assessed in a test performed at 160 °C (see Figure S7). During the latter test, a constant $C_3H_6$ concentration (500 ppm) was assured. The consumption rate of oxygen was evaluated observing the appearance of CO and $CO_2$ related to the catalytic oxidation of propylene. This test evidenced an increasing rate of oxygen consumption when propylene was in high excess. Whereas, when the amount of $O_2$ was above 1 vol.%, its consumption rate did not evidence important variations. Interestingly, this relatively constant consumption suggests that the catalytic surface may be saturated of oxygen. Interestingly, this result highlights that the catalytic activity of the $MnCu_{15}$ in the oxidation of propylene remains practically unvaried when the content of $O_2$ in the inlet changes between 1 and 10 vol.%. On the other hand, the higher consumption rate occurring when 1 vol.% of $O_2$ was inserted may suggest that other catalytic phenomena could be occurring, *e.g.* improved adsorption of propylene in competitive sites or the better availability of lattice oxygen like in a Mars-van Krevelen reaction mechanism. Actually, the latter case seems probable, since the insertion of Cu in the framework of $Mn_2O_3$ (as demonstrated by the XRD analyses, *vide supra*) improved the mobility of lattice oxygen species, in accordance with the $H_2$ and soot TPR characterizations.

**Simultaneous Oxidation of Soot and Propylene** With comparison purposes, the catalytic abatement of propylene was performed, using a catalytic bed that did not contain any soot. Figure 12ab evidences the CO and $CO_2$ signals observed during the propylene catalytic oxidation test (red dashed line), as well as those measured during the simultaneous soot-propylene abatement (black solid line). As observed in the Figure 12a, the $CO_2$ profile obtained during the soot-VOC simultaneous test seems to be the overlapping signals of the single catalytic tests, *i.e.* the sum of the signals observed during the oxidation of $C_3H_6$ and the soot+$C_3H_6$ separate tests. Interestingly, these results suggest that both the oxidation of propylene and soot can take place simultaneously without any evident negative effect of one process above the other. The Figure 12c shows the soot catalytic conversions observed during the single-soot oxidation, and those observed during the mixed soot-VOC catalytic oxidation test. Interestingly, it was observed that a higher amount of soot was oxidized during the simultaneous soot-VOC abatement test (at *ca.* 350 °C), compared to the one consumed during the soot oxidation test.

On the other hand, the results obtained when the simultaneous oxidation of soot and $C_3H_6$ was assessed in presence of 5 vol.% of $H_2O$ are shown in Figure 13. Similar to the test described previously, the first $CO_2$ signal (see Figure 13a) appeared at the same temperatures observed during the oxidation of propylene in presence of water (red dashed line). Therefore, it was assigned to the oxidation of $C_3H_6$ taking place independently from the oxidation of soot. At T > 280 °C, the $CO_2$ profile shape observed is comparable to those observed during the oxidation of soot over the prepared manganese oxides with peaks maxima occurring at similar temperatures (see Figure 6a). However, the $CO_2$ and CO signals observed at ca. 600 °C in Figure 13ab, indicate that an increased amount of the soot is being converted by means of thermal oxidation. Therefore, according to the literature this

**FIGURE 12** Amount of $CO_2$ (Section A) and CO (Section B) as a function of the temperature, produced during the tests for the oxidation of propylene and soot + propylene in "loose contact" conditions. Section C: Soot conversion (%) curves in presence (black solid line) and in absence of $C_3H_6$ (blue dashed line) as a function of the temperature.

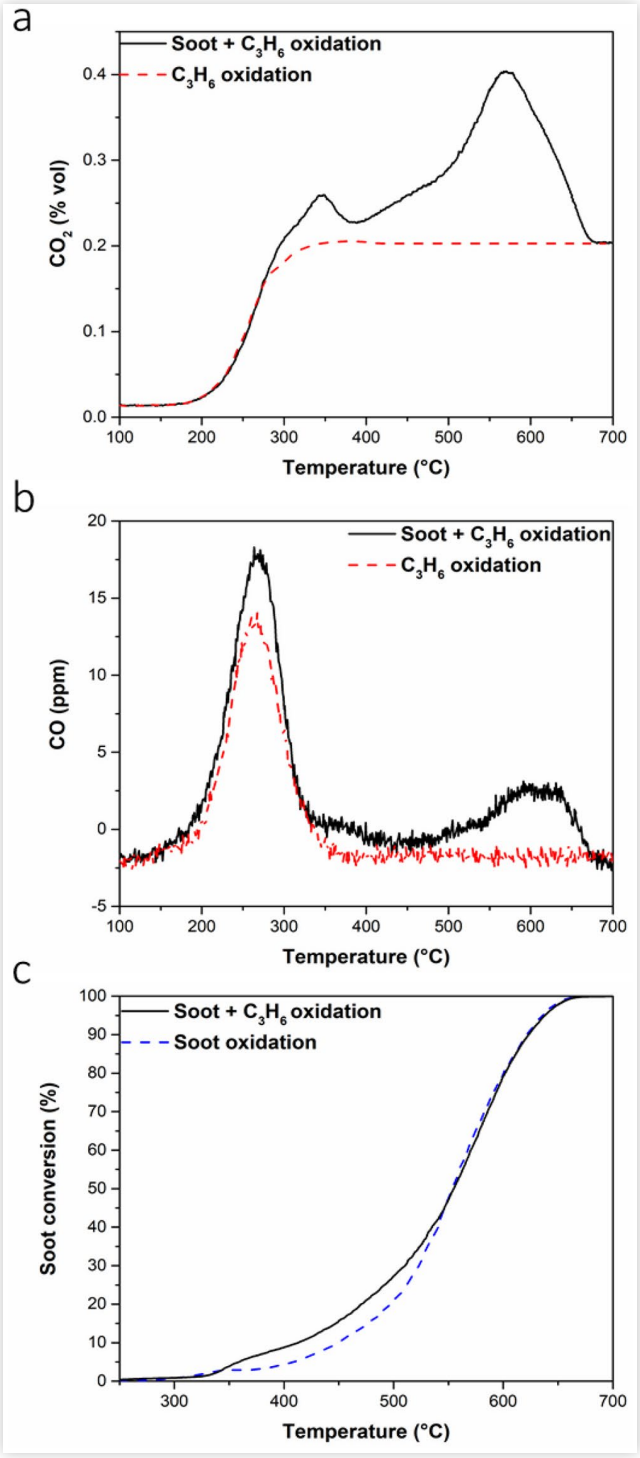


**FIGURE 13** Amount of $CO_2$ (Section A) and CO (Section B) as a function of the temperature, produced during the oxidation of propylene and soot + propylene simultaneously in "loose contact" conditions with a 5 vol.% of $H_2O$ in the stream. Section C: Soot conversion (%) curves in presence (black solid line) and in absence of $C_3H_6$ (orange dashed line) as a function of the temperature with 5 vol.% of $H_2O$ in the stream.

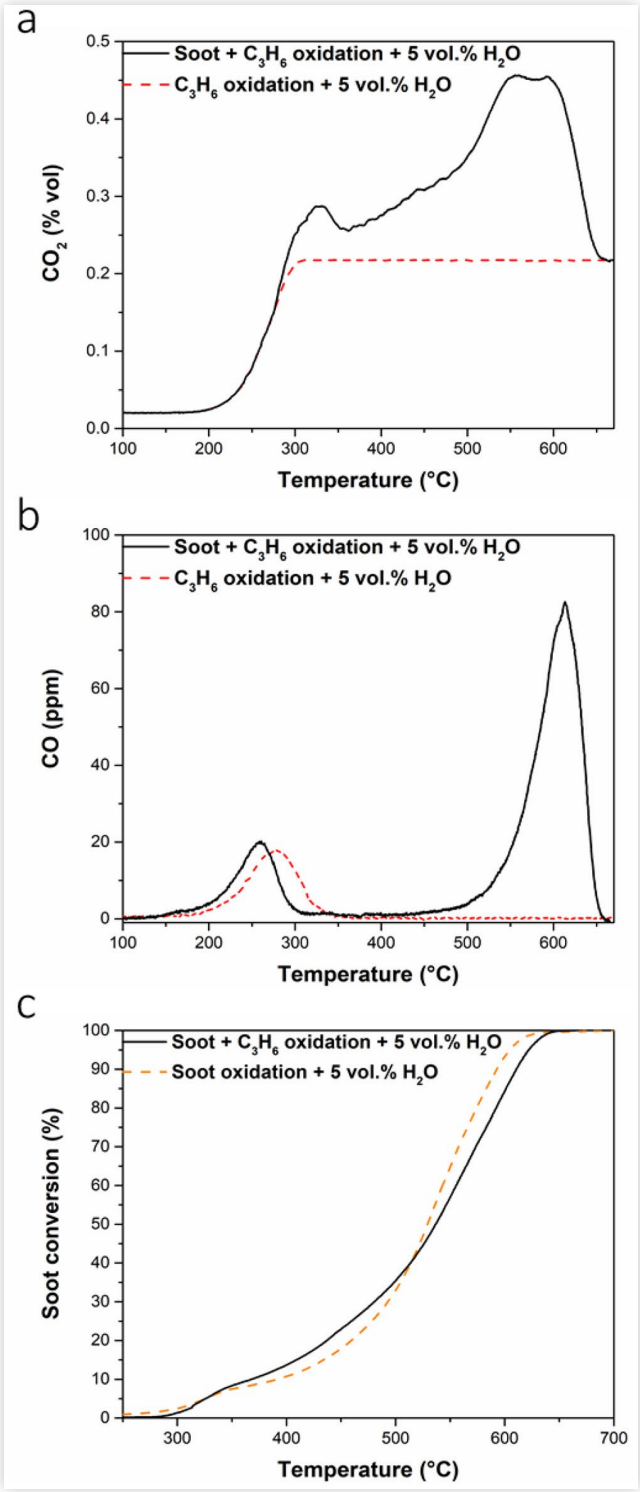

was ascribed to the presence of water in the stream that was observed to worsen the conversion of soot, thus probably promoting the deactivation of the catalyst [34]. Remarkably, the amount of soot converted (black solid line) below *ca.* 515 °C seems higher compared to the case in which propylene is not present in the system (see Figure 13c). This finding coincides with the results observed in Figure 12c. As discussed previously, the oxidation taking place in that temperature range was ascribed to the oxidation of soot particles in "tight" contact with the catalyst. In fact, according to the literature, the rate of soot oxidation under "tight" contact conditions may be enhanced in the presence of VOCs [39, 40]. These results suggest that a beneficial interaction could be taking place between the mechanisms of the soot oxidation reaction over the catalytic surface, and the ongoing catalytic oxidation of $C_3H_6$. Actually, previous research [39] demonstrated that the ignition of the exothermal oxidation of propylene may induce the abatement of soot at low temperatures. In this sense, the exothermal oxidation reaction of propylene could be generating local increases of the temperature in the catalytic surface that may initiate the oxidation of some soot in the low temperature range.

As a whole, the results supply strong evidence for assuming that the oxidation of propylene takes place in spite of the presence of soot in the reactor. Furthermore, the results of the simultaneous soot-VOC oxidation tests highlight that the catalytic reaction for propylene oxidation may assist the oxidation of soot by allowing its partial elimination at lower temperatures than those required when the VOC is not present in the gaseous inlet.

# Conclusions

In this research work, a set of doped manganese oxide ($Mn_2O_3$) catalysts were prepared by means of the sol-gel synthesis using citric acid. The samples prepared were doped with Cu and/or Fe (namely, $MnCu_{15}$, $MnFe_{15}$ and $MnCu_{7.5}Fe_{7.5}$). As a whole, the experimental data obtained for soot oxidation highlighted the parent $Mn_2O_3$ as the most performing catalyst. The catalytic activity of the aforementioned oxide showed a good stability in oxidation tests after being subject to a severe aging treatment and, as well, when humidity (*ca.* 5 vol.%) was present in the stream. The catalytic performance in the oxidation of soot was correlated to the ratio between the relative amounts of $Mn^{3+}/Mn^{2+}$ species on the catalyst's surface. Thus, highlighting the significative role of reducible manganese species in the oxidation of soot.

On the other hand, the catalyst $MnCu_{15}$, showed the best overall performance in the oxidation of propylene. The reproducibility of the catalytic performance was verified in consecutive tests. Its catalytic stability was confirmed in a 7 h TOS experiment with swinging temperature conditions. As well, the catalyst's performance showed almost no deactivation when 5 vol.% of humidity was present in the gaseous stream. The catalytic enhancement was effectively correlated to the improved reducibility caused by the insertion of Cu in the structure of the $Mn_2O_3$.

Finally, the tests for the simultaneous oxidation of soot and propylene either in dry or humid conditions (5 vol.% of $H_2O$), evidenced the fairly stable catalytic performance of the $Mn_2O_3$, since the oxidation of both $C_3H_6$ and soot occurred simultaneously. Surprisingly, the results showed that the oxidation of soot particles seems to be enhanced when propylene is being oxidized, thus suggesting that soot oxidation could be assisted by the propylene oxidation reaction mechanism.

# References


1. European Parliament and Council, "Directive 2008/50/EC of the European Parliament and of the Council of 21 May 2008 on Ambient Air Quality and Cleaner Air for Europe," 2008, https://eur-lex.europa.eu/legal-content/EN/TXT/?qid=1600695099487&uri=CELEX:02008L0050-20150918, accessed Jan. 2021.
2. United States Environmental Protection Agency, "Particulate Matter (PM) Implementation Regulatory Actions," 2019, https://www.epa.gov/pm-pollution/particulate-matter-pm-implementation-regulatory-actions, .
3. Zbarcea, O., Scarpete, D., and Vrabie, V., "Environmental Pollution by Diesel Engines. Part II: A Literature Review Regarding HC, CO, CO 2 and Soot Emissions," Report, "Dunărea de Jos" University of Galati, Romania, 2016.
4. Mohankumar, S. and Senthilkumar, P., "Particulate Matter Formation and Its Control Methodologies for Diesel Engine: A Comprehensive Review," *Renewable and Sustainable Energy Reviews* 80 (2017): 1227-1238. https://doi.org/10.1016/j.rser.2017.05.133.
5. Gupta, T. and Kumar Singh, D., "Organic Species Emitted as a Part of Combustion Residue: Fate and Transformation in the Ambient Air," *Journal or Energy and Environmental Sustainability* 1 (2016, 2016): 10-18, doi:10.47469/JEES.2016.v01.100002.
6. Wasalathanthri, N.D., SantaMaria, T.M., Kriz, D.A., Dissanayake, S.L. et al., "Mesoporous Manganese Oxides for NO2 Assisted Catalytic Soot Oxidation," *Applied Catalysis B: Environmental* 201 (2017): 543-551. https://doi.org/10.1016/j.apcatb.2016.08.052.
7. Piumetti, M., Bensaid, S., Andana, T., Russo, N. et al., "Cerium-Copper Oxides Prepared by Solution Combustion Synthesis for Total Oxidation Reactions: From Powder Catalysts to Structured Reactors," *Applied Catalysis B: Environmental* 205 (2017): 455-468. https://doi.org/10.1016/j.apcatb.2016.12.054.
8. Ranji-Burachaloo, H., Masoomi-Godarzi, S., Khodadadi, A.A., and Mortazavi, Y., "Synergetic Effects of Plasma and Metal Oxide Catalysts on Diesel Soot Oxidation," *Applied Catalysis B: Environmental* 182 (2016): 74-84. https://doi.org/10.1016/j.apcatb.2015.09.019.
9. Haynes, W.M., *CRC Handbook of Chemistry and Physics : A Ready-Reference Book of Chemical and Physical Data, 95th edition* (CRC Press, 2014), ISBN:1482208687, 9781482208689
10. Piumetti, M., van der Linden, B., Makkee, M., Miceli, P., et al., "Contact Dynamics for a Solid-Solid Reaction Mediated by Gas-Phase Oxygen: Study on the Soot Oxidation Over Ceria-Based Catalysts," *Applied Catalysis B: Environmental* 199:96-107, 2016, https://doi.org/10.1016/j.apcatb.2016.06.006.
11. Neeft, J.P.A., Makkee, M., and Moulijn, J.A., "Catalysts for the Oxidation of Soot from Diesel Exhaust Gases. I. An

Exploratory Study," *Applied Catalysis B: Environmental* 8, no. 1 (1996): 57-78. https://doi.org/10.1016/0926-3373(95)00057-7.

12. Andana, T., Piumetti, M., Bensaid, S., Russo, N. et al., "Nanostructured Ceria-Praseodymia Catalysts for Diesel Soot Combustion," *Applied Catalysis B: Environmental* 197 (2016): 125-137. https://doi.org/10.1016/J.APCATB.2015.12.030.
13. Dosa, M., Piumetti, M., Bensaid, S., Andana, T. et al., "Novel Mn-Cu-Containing CeO2 Nanopolyhedra for the Oxidation of CO and Diesel Soot: Effect of Dopants on the Nanostructure and Catalytic Activity," *Catalysis Letters* 148, no. 1 (2018): 298-311. https://doi.org/10.1007/s10562-017-2226-y.
14. Piumetti, M., Fino, D., and Russo, N., "Mesoporous Manganese Oxides Prepared by Solution Combustion Synthesis as Catalysts for the Total Oxidation of VOCs," *Applied Catalysis B: Environmental* 163 (2015): 277-287. https://doi.org/10.1016/j.apcatb.2014.08.012.
15. Shannon, R.D., "Revised Effective Ionic Radii and Systematic Studies of Interatomic Distances in Halides and Chalcogenides," *Acta Crystallographica Section A* 32, no. 5 (1976): 751-767. https://doi.org/10.1107/S0567739476001551.
16. Santos, V.P., Pereira, M.F.R., Órfão, J.J.M., and Figueiredo, J.L., "The Role of Lattice Oxygen on the Activity of Manganese Oxides Towards the Oxidation of Volatile Organic Compounds," *Applied Catalysis B: Environmental* 99, no. 1-2 (2010): 353-363. https://doi.org/10.1016/j.apcatb.2010.07.007.
17. Delimaris, D. and Ioannides, T., "VOC Oxidation Over MnOx-CeO2 Catalysts Prepared by a Combustion Method," *Applied Catalysis B: Environmental* 84, no. 1-2 (2008): 303-312. https://doi.org/10.1016/j.apcatb.2009.02.003.
18. Marin Figueredo, M.J., Andana, T., Bensaid, S., Dosa, M. et al., "Cerium-Copper-Manganese Oxides Synthesized via Solution Combustion Synthesis (SCS) for Total Oxidation of VOCs," *Catalysis Letters* 150, no. 6 (2020): 1821-1840. https://doi.org/10.1007/s10562-019-03094-x.
19. Leith, I.R. and Howden, M.G., "Temperature-Programmed Reduction of Mixed Iron-Manganese Oxide Catalysts in Hydrogen and Carbon Monoxide," *Applied Catalysis* 37, no. C (1988): 75-92. https://doi.org/10.1016/S0166-9834(00)80752-6.
20. Li, T., Yang, Y., Zhang, C., Tao, Z. et al., "Effect of Manganese Incorporation Manner on an Iron-Based Catalyst for Fischer-Tropsch Synthesis," *Journal of Natural Gas Chemistry* 16, no. 3 (2007): 244-251. https://doi.org/10.1016/S1003-9953(07)60055-3.
21. Gandhe, A.R., Rebello, J.S., Figueiredo, J.L., and Fernandes, J.B., "Manganese Oxide OMS-2 as an Effective Catalyst for Total Oxidation of Ethyl Acetate," *Applied Catalysis B: Environmental* 72, no. 1-2 (2007): 129-135. https://doi.org/10.1016/j.apcatb.2006.10.017.
22. Li, Z., Meng, M., Zha, Y., Dai, F. et al., "Highly Efficient Multifunctional Dually-Substituted Perovskite Catalysts La 1-xK xCo 1-yCu yO 3-δ Used for Soot Combustion, NOx Storage and Simultaneous NOx-Soot Removal," *Applied Catalysis B: Environmental* 121-122 (2012): 65-74. https://doi.org/10.1016/j.apcatb.2012.03.022.
23. Spinicci, R. and Tofanari, A., "Characterization of Catalysts for Methane-Coupling by Means of Temperature Programmed Desorption," *Catalysis Today* 6, no. 4 (1990): 473-479. https://doi.org/10.1016/0920-5861(90)85041-L.
24. Biesinger, M.C., Payne, B.P., Grosvenor, A.P., Lau, L.W.M. et al., "Resolving Surface Chemical States in XPS Analysis of First Row Transition Metals, Oxides and Hydroxides: Cr, Mn, Fe, Co and Ni," *Applied Surface Science* 257, no. 7 (2011): 2717-2730. https://doi.org/10.1016/j.apsusc.2010.10.051.
25. Moulder, J.F., Stickle, W.F., Sobol, P.E., and Bomben, K.D., in: Chastain, J. (Eds), *Handbook of X-ray Photoelectron Spectroscopy*, (Perkin-Elmer Corporation, Physical Electronics Division, 1992), ISBN:0962702625, 9780962702624.
26. Kim, S.C. and Shim, W.G., "Catalytic Combustion of VOCs Over a Series of Manganese Oxide Catalysts," *Applied Catalysis B: Environmental* 98, no. 3-4 (2010): 180-185. https://doi.org/10.1016/j.apcatb.2010.05.027.
27. Yamashita, T. and Hayes, P., "Analysis of XPS Spectra of Fe 2+ and Fe 3+ Ions in Oxide Materials," *Applied Surface Science* 254, no. 8 (2008): 2441-2449. https://doi.org/10.1016/j.apsusc.2007.09.063.
28. Biesinger, M.C., Lau, L.W.M., Gerson, A.R., and Smart, R.S.C., "Resolving Surface Chemical States in XPS Analysis of First Row Transition Metals, Oxides and Hydroxides: Sc, Ti, V, Cu and Zn," *Applied Surface Science* 257, no. 7 (2010): 887-898. https://doi.org/10.1016/j.apsusc.2010.10.051.
29. Kundakovic, L. and Flytzani-Stephanopoulos, M., "Reduction Characteristics of Copper Oxide in Cerium and Zirconium Oxide Systems," *Applied Catalysis A: General* 171, no. 1 (1998): 13-29. https://doi.org/10.1016/S0926-860X(98)00056-8.
30. Liu, W. and Flytzani-Stephanopoulos, M., "Total Oxidation of Carbon-Monoxide and Methane over Transition Metal-Fluorite Oxide Composite Catalysts: II. Catalyst Characterization and Reaction-Kinetics," *Journal of Catalysis* 153, no. 2 (1995): 317-332. https://doi.org/10.1006/jcat.1995.1133.
31. Piumetti, M., Bensaid, S., Russo, N., and Fino, D., "Nanostructured Ceria-Based Catalysts for Soot Combustion: Investigations on the Surface Sensitivity," *Applied Catalysis B: Environmental* 165 (2015): 742-751. https://doi.org/10.1016/j.apcatb.2014.10.062.
32. Mars, P., and van Krevelen, D.W., "Oxidations Carried Out by Means of Vanadium Oxide Catalysts," *Chemical Engineering Science* 3:41-59, 1954, https://doi.org/10.1016/S0009-2509(54)80005-4.
33. Christensen, J.M., Grunwaldt, J.D., and Jensen, A.D., "Effect of NO2 and Water on the Catalytic Oxidation of Soot," *Applied Catalysis B: Environmental* 205 (2017): 182-188. https://doi.org/10.1016/j.apcatb.2016.12.024.
34. Peralta, M.A., Milt, V.G., Cornaglia, L.M., and Querini, C.A., "Stability of Ba,K/CeO2 Catalyst During Diesel Soot Combustion: Effect of Temperature, Water, and Sulfur Dioxide," *Journal of Catalysis* 242, no. 1 (2006): 118-130. https://doi.org/10.1016/j.jcat.2006.05.025.
35. Morales, M.R., Barbero, B.P., and Cadús, L.E., "Evaluation and Characterization of Mn-Cu Mixed Oxide Catalysts for Ethanol Total Oxidation: Influence of Copper Content," *Fuel* 87, no. 7 (2008): 1177-1186. https://doi.org/10.1016/j.fuel.2007.07.015.
36. Morales, M.R., Barbero, B.P., and Cadús, L.E., "Total Oxidation of Ethanol and Propane Over Mn-Cu Mixed

Oxide Catalysts," *Applied Catalysis B: Environmental* 67, no. 3-4 (2006): 229-236. https://doi.org/10.1016/j.apcatb.2006.05.006.

37. Fang, J., Chen, X., Xia, Q., Xi, H. et al., "Effect of Relative Humidity on Catalytic Combustion of Toluene over Copper Based Catalysts with Different Supports," *Chinese Journal of Chemical Engineering* 17, no. 5 (2009): 767-772. https://doi.org/10.1016/S1004-9541(08)60275-X.
38. Li, W.B., Wang, J.X., and Gong, H., "Catalytic Combustion of VOCs on Non-Noble Metal Catalysts," *Catalysis Today* 148, no. 1-2 (2010): 81-87. https://doi.org/10.1016/j.cattod.2009.03.007.
39. Aouad, S., Abi-Aad, E., and Aboukaïs, A., "Simultaneous Oxidation of Carbon Black and Volatile Organic Compounds Over Ru/CeO2 Catalysts," *Applied Catalysis B: Environmental* 88, no. 3-4 (2009): 249-256. https://doi.org/10.1016/j.apcatb.2008.10.002.
40. Godoy, M., Banús, E., Sanz, O., Montes, M. et al., "Stacked Wire Mesh Monoliths for the Simultaneous Abatement of VOCs and Diesel Soot," *Catalysts* 8, no. 1 (2018): 1-16. https://doi.org/10.3390/catal8010016.

## Contact Information

**Miguel J. Marin F. (first-author)**
Department of Applied Science and Technology
Politecnico di Torino
Corso Duca degli Abruzzi 24, 10129 Torino, Italy
miguel.marinfigueredo@polito.it

**Clarissa Cocuzza**
Department of Applied Science and Technology
Politecnico di Torino
Corso Duca degli Abruzzi 24, 10129 Torino, Italy
clarissa.cocuzza@polito.it

**Marco Piumetti (corresponding author)**
Department of Applied Science and Technology
Politecnico di Torino
Corso Duca degli Abruzzi 24, 10129 Torino, Italy
marco.piumetti@polito.it

**Samir Bensaid**
Department of Applied Science and Technology
Politecnico di Torino
Corso Duca degli Abruzzi 24, 10129 Torino, Italy
samir.bensaid@polito.it

**Nunzio Russo**
Department of Applied Science and Technology
Politecnico di Torino
Corso Duca degli Abruzzi 24, 10129 Torino, Italy
nunzio.russo@polito.it

**Debora Fino**
Department of Applied Science and Technology
Politecnico di Torino
Corso Duca degli Abruzzi 24, 10129 Torino, Italy
debora.fino@polito.it

## Acknowledgments

This project has received funding from the European Union's Horizon 2020 research and innovation programme under grant agreement No 768692

# Appendix

## Supporting Figures

**FIGURE S1** $Mn^{x+}$ species relative abundances as calculated by the deconvolution of the Mn (2*p*) spectra of the catalysts.

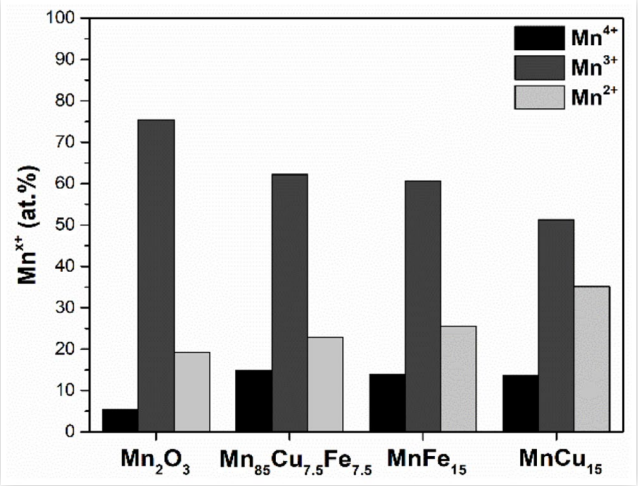

**FIGURE S2** Relative abundance of chemisorbed ($O_\alpha$) and lattice ($O_\beta$) oxygen species in the catalysts calculated after deconvolution of the corresponding O (1s) spectra.

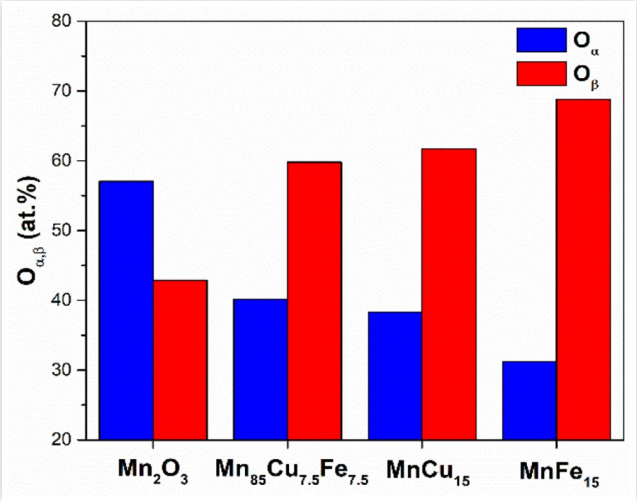


**FIGURE S3** Soot catalytic oxidation rates as a function of the relative amount of the $Mn^{2+}$ species.

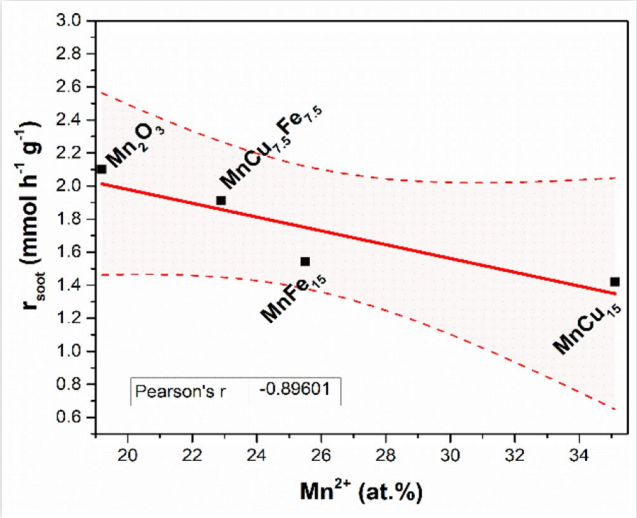

**FIGURE S4** Amount of $CO_2$ (Sections A,C)and CO (Sections B,D) produced and conversion (%) curves (Section E) as a function of the temperature observed in the catalytic oxidation of soot, performed in "loose" contact conditions over the $Mn_2O_3$ and the $MnCu_{7.5}Fe_{7.5}$ catalysts subject to aging treatment.

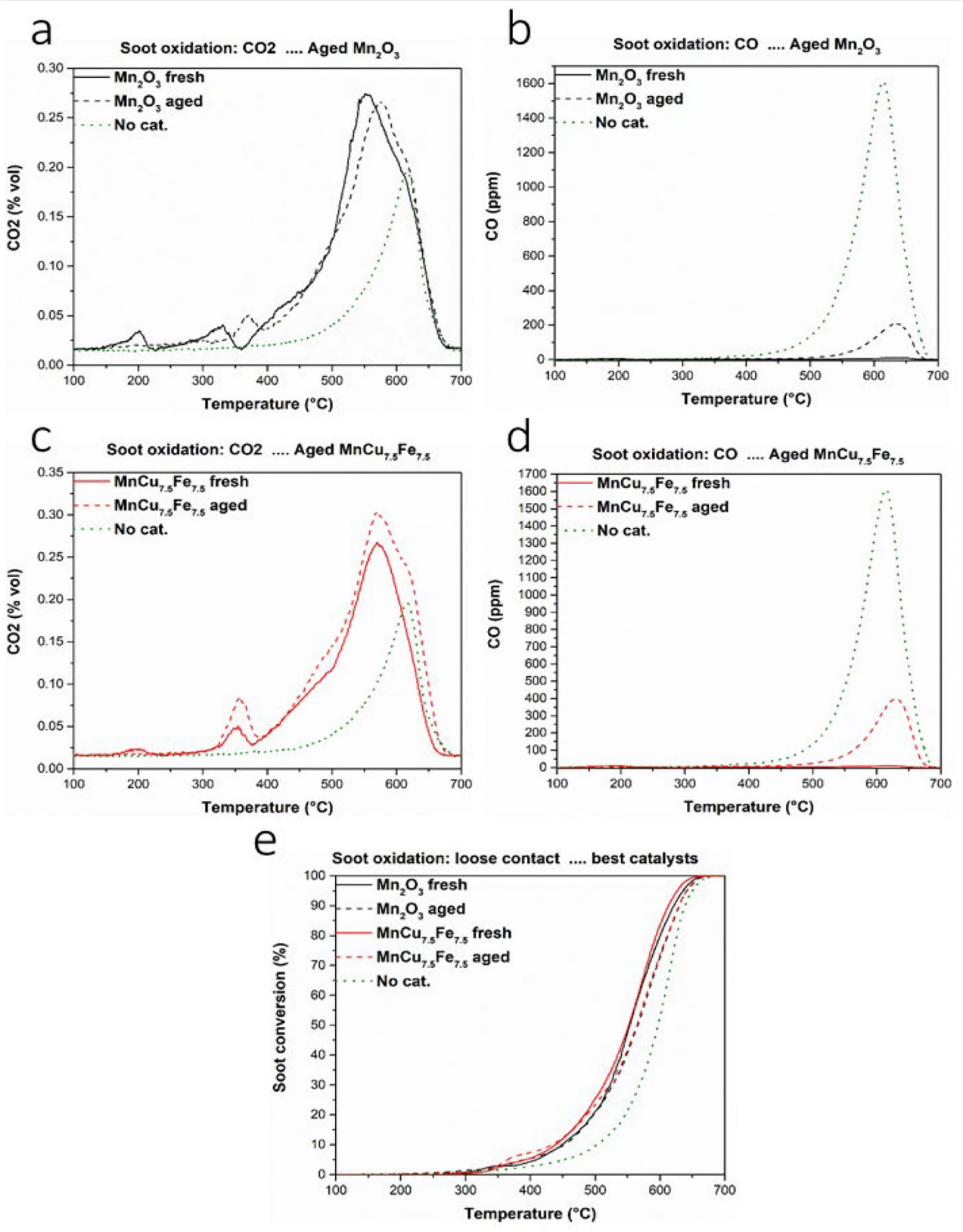

**FIGURE S5** Reproducibility of the overall catalytic performance over the $MnCu_{15}$ catalyst after two consecutive operative runs.

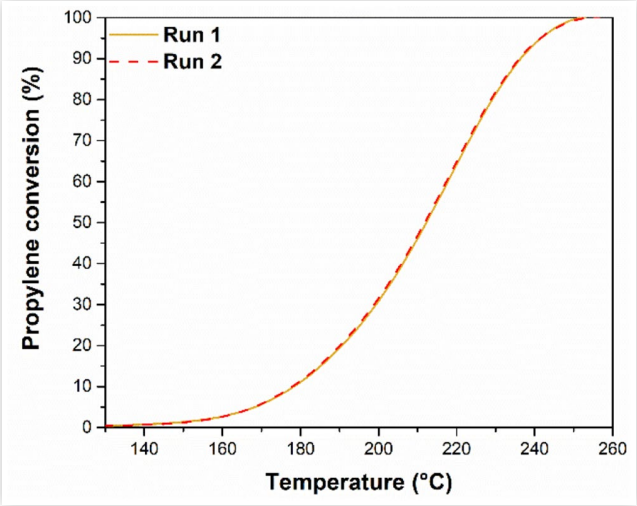


**FIGURE S6** Reaction rates of $C_3H_6$ between 150 °C and 180 °C as a function of the propylene content fed in the reactor inlet.

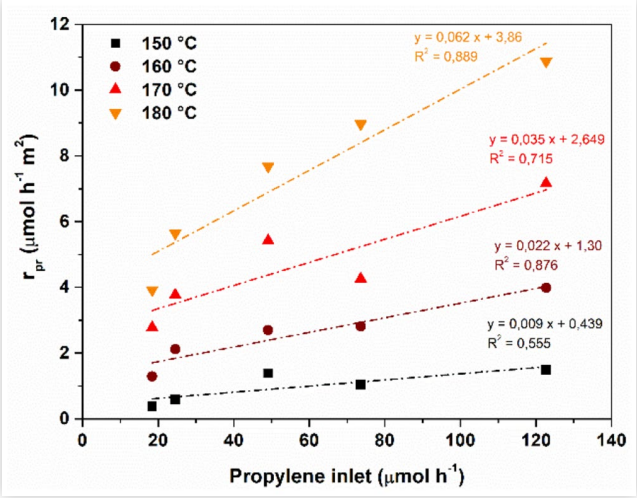

**FIGURE S7** Oxygen catalytic oxidation rates at 160 °C as a function of the oxygen content fed in the reactor inlet.

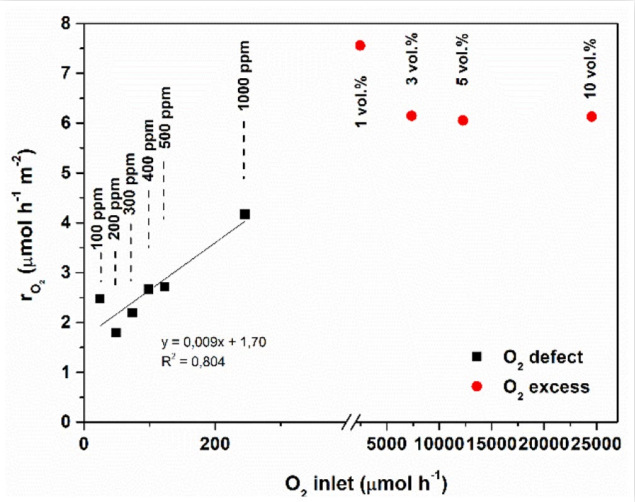




ISSN 0148-7191